Computer Methods in Biomechanics and Biomedical Engineering

Publication details, including instructions for authors and subscription information:
http://www.tandfonline.com/loi/gcmb20

Generating fibre orientation maps in human heart models using Poisson interpolation

Jonathan Wong [a] & Ellen Kuhl [a b c]

[a] Department of Mechanical Engineering, Stanford University, Stanford, CA, 94305, USA

[b] Department of Bioengineering, Stanford University, Stanford, CA, 94305, USA

[c] Department of Cardiothoracic Surgery, Stanford University, Stanford, CA, 94305, USA

Version of record first published: 05 Dec 2012.

To cite this article: Jonathan Wong & Ellen Kuhl (2012): Generating fibre orientation maps in human heart models using Poisson interpolation, Computer Methods in Biomechanics and Biomedical Engineering, DOI:10.1080/10255842.2012.739167

To link to this article: http://dx.doi.org/10.1080/10255842.2012.739167

Computer Methods in Biomechanics and Biomedical Engineering
iFirst article, 2012, 1–10

Generating fibre orientation maps in human heart models using Poisson interpolation

Jonathan Wong[a]* and Ellen Kuhl[a,b,c]

[a]*Department of Mechanical Engineering, Stanford University, Stanford, CA 94305, USA;* [b]*Department of Bioengineering, Stanford University, Stanford, CA 94305, USA;* [c]*Department of Cardiothoracic Surgery, Stanford University, Stanford, CA 94305, USA*

(*Received 15 June 2012; final version received 9 October 2012*)

Smoothly varying muscle fibre orientations in the heart are critical to its electrical and mechanical function. From detailed histological studies and diffusion tensor imaging, we now know that fibre orientations in humans vary gradually from approximately -70° in the outer wall to $+80^\circ$ in the inner wall. However, the creation of fibre orientation maps for computational analyses remains one of the most challenging problems in cardiac electrophysiology and cardiac mechanics. Here, we show that Poisson interpolation generates smoothly varying vector fields that satisfy a set of user-defined constraints in arbitrary domains. Specifically, we enforce the Poisson interpolation in the weak sense using a standard linear finite element algorithm for scalar-valued second-order boundary value problems and introduce the feature to be interpolated as a global unknown. User-defined constraints are then simply enforced in the strong sense as Dirichlet boundary conditions. We demonstrate that the proposed concept is capable of generating smoothly varying fibre orientations, quickly, efficiently and robustly, both in a generic bi-ventricular model and in a patient-specific human heart. Sensitivity analyses demonstrate that the underlying algorithm is conceptually able to handle both arbitrarily and uniformly distributed user-defined constraints; however, the quality of the interpolation is best for uniformly distributed constraints. We anticipate our algorithm to be immediately transformative to experimental and clinical settings, in which it will allow us to quickly and reliably create smooth interpolations of arbitrary fields from data-sets, which are sparse but uniformly distributed.

Keywords: feature-based interpolation; Poisson equation; finite element method; anisotropy; fibre orientation; cardiac electrophysiology

1. Introduction

The structural architecture of the heart is one of the most important factors to healthy pump function (Kumar et al. 2005). Although many geometric factors such as shape, thickness and size play a critical role in disease diagnosis, the correct alignment of cardiac muscle fibres is crucial for proper choreography of cardiac muscle contraction (Opie 2003). In fact, many cardiac disorders or traumatic events induce cardiac fibre misalignment, which may cyclically reduce cardiac function and lead to further disorganisation (Libby et al. 2007). For example, in response to cardiac infarctions, residual fibres are secreted to structurally stabilise the heart. However, these fibres lose organisation and may actually form nodes of orthogonal myofibre intersection or contact which impede proper cardiac function (Sosnovik et al. 2009). Other pathologies such as myocardial fibrosis are also known to modify organised fibre orientation, ultimately impairing both electrical and mechanical function (Schmitt et al. 2009). Therefore, it is imperative for computational models of the heart to include proper fibre orientation distributions to accurately predict the electrical and mechanical function of the heart in health and disease.

Figure 1 illustrates the characteristic microstructure of the heart by means of the fibre direction **f**, the sheet plane normal **s** and their normal **m**. Fortunately, the overall structural alignment of the human heart is well characterised in the literature (Streeter and Hanna 1973), in which fibres have been reported to vary transmurally from approximately -70° in the epicardium, the outer wall, to $+80^\circ$ in the endocardium, the inner wall (Arts et al. 2001; Geerts et al. 2002). However, along the septal wall, the right endocardium displays a fibre orientation of approximately -70°. Although there is a wide agreement on these fibre orientations in the epicardial and endocardial walls, there is no generally accepted concept to assign these fibre orientations to realistic anatomical computer models of the human heart. Simplified attempts represent the two ventricles as nested, truncated ellipsoids and allow for an analytical characterisation of the fibre orientation distribution (Göktepe and Kuhl 2010). Other techniques rely on complex projections and use least squares fitting to generate a continuum description of fibre orientations (Toussaint et al. 2010a). Recent attempts have adopted a

*Corresponding author. Email: jonjwong@alumni.stanford.edu

ISSN 1025-5842 print/ISSN 1476-8259 online

http://dx.doi.org/10.1080/10255842.2012.739167
http://www.tandfonline.com

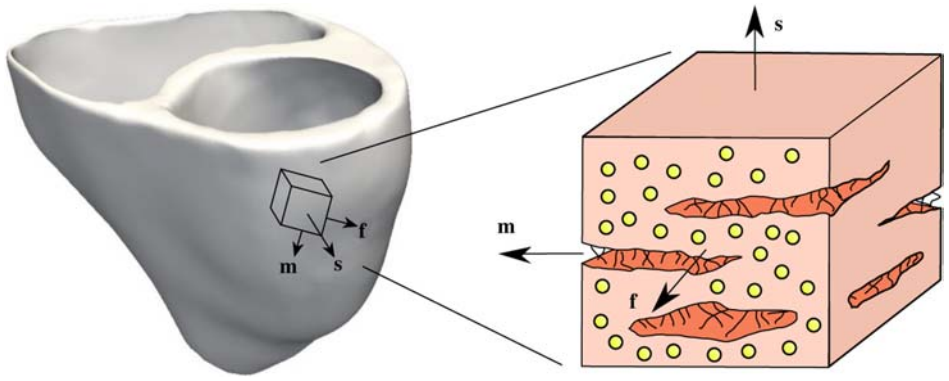

Figure 1. Characteristic microstructure in the human heart. Fibre directions **f** vary transmurally from approximately -70° in the epicardium, the outer wall, to $+80^\circ$ in the endocardium, the inner wall. Fibre vectors **f** and sheet vectors **m** locally span the sheet plane, with the sheet plane normal **s** pointing outwards, approximately orthogonal to the epicardial wall.

geometrically based approach to mitigate some of the difficulties in determining approximate fibre orientations in irregular geometries (Takayama et al. 2008).

When heart fibre orientations were first characterised, the goal was to identify an analytical description for a single ellipsoid representing the left ventricle (Nielsen et al. 1991). Initially, Hammer projections served to map a real heart geometry onto an idealised prolate spheroidal ellipsoid to create a mathematical model of the fibre directions in the heart. A more recent variation of this technique has been applied to diffusion tensor image interpolation (Toussaint et al. 2010a). The irregular geometry is first projected to a prolate spheroid coordinate system, and then smoothed using an averaging kernel and least squares approach to generate an interpolation in the idealised domain. In addition, some groups use least squares techniques to fit the experimentally measured fibre directions to an approximated geometrical mesh (Costa et al. 1996; Toussaint et al. 2010a). The fibre directions from a least squares approach can then be interpolated onto element centroids, nodes or integration points of the finite element mesh by using the corresponding finite element shape functions. For more complex interpolating schemes, different weights can be assigned to the individual interpolants. Most recently, a geometrical-based approach was proposed to provide sketch-based methods for generating layered fibre structures for the heart (Takayama et al. 2008).

Unfortunately, there are several essential drawbacks in using ellipsoid, projected or least squares techniques. For example, some difficulties may arise when trying to determine proper projections for mapping a non-ellipsoidal geometry onto an idealised ellipsoidal representation of the heart. With the relative accessibility of different 3D imaging modalities today, we can attain patient-specific heart geometries relatively easily (Kotikanyadanam et al. 2010). In general, these geometries do not look like ellipsoids, and there may be inherent singularities when mapping each ventricle onto an idealised ellipsoid, in particular in the septal region and close to the apex (Toussaint et al. 2010b). Of all existing techniques, least squares techniques might therefore be best suited to fit experimentally measured data. However, they may require some fine-tuning to create sufficiently continuous fibre orientations. In addition, they typically require a sufficiently complete set of experimental data.

Overall, the above challenges mainly add complexity to designating fibre orientation maps throughout the heart. Here, we propose a novel fibre interpolation concept, which significantly reduces the complexity of generating fibre orientation distributions within arbitrary geometries. In addition, it allows for more flexibility with regard to mesh refinement and is easily accessible and intuitive to the field of computational biomechanics. The underlying approach is adopted from feature-based interpolation techniques (Yang et al. 2012) used in computer graphics (Fisher et al. 2007), and is conceptually similar to sketch-based methods (Takayama et al. 2008). However, our approach is finite element based and provides a straightforward refinement to properly describe both ventricles of the heart, while maintaining a continuous fibre orientation distribution. The key to reducing complexity, ironically, is to reformulate the orientation of the heart from an explicit representation of measured or mathematically parametrised orientations to a more implicit one. This eliminates having to make difficult and subjective assumptions by simply calculating the fibre orientation as the solution to a boundary value problem. Although the concept is inherently applicable to different types of boundary value problems, here we use the Poisson equation as an interpolation method to solve for our designated fibre angle orientation distribution.

This paper is organised into four additional sections. First, in Section 2, we introduce the Poisson interpolation, the generation of local cardiac coordinate systems and the creation of Dirichlet boundary conditions, which serve as

the basis for the fibre interpolation. Then, in Section 3, we illustrate the concept of the Poisson interpolation on an idealised geometry to quantitatively compare it with an analytical fibre orientation and on a patient-specific geometry to demonstrate the generality of the underlying scheme. We also perform two sensitivity analyses to identify the amount of information required to generate smooth fibre orientation maps. This mimics the potential to interpolate fibre orientation distributions using experimentally acquired data. Finally, in Section 4, we discuss the merits and limitations of our algorithm and highlight future possible avenues.

2. Methods

2.1 Poisson interpolation of scalar-valued feature

The key idea of our fibre orientation algorithm is to generate a smooth coordinate-free fibre interpolation using algorithms from computer graphics motivated by feature-based interpolation. In essence, we solve the following Poisson equation for the scalar-valued feature θ,

$$\text{div}(\mathbf{K}\cdot\nabla\theta) = 0 \quad \text{in} \quad \mathcal{B} \tag{1}$$

for given Dirichlet boundary conditions

$$\theta = \bar{\theta} \quad \text{on} \quad \partial\mathcal{B}_\theta. \tag{2}$$

For isotropic constant diffusion coefficients, $\mathbf{K} = K\mathbf{I}$, the Poisson equation reduces to the homogeneous Laplacian, $\Delta\theta = 0$, generating a smooth linear interpolation of the feature θ across the cardiac domain $\mathcal{B}$. To solve the underlying partial differential Equation (1), we transform it into its weak form, integrate it over the domain $\mathcal{B}$, discretise it with linear tetrahedral elements and solve the resulting system with the corresponding Dirichlet boundary conditions (2). This implies that we solve the fibre interpolation (1) in a weak sense, while we enforce the set of user-defined constraints (2) in a strong sense. For the finite element solution, we can adopt any standard finite element program for linear diffusion or thermal problems, and interpret the scalar-valued feature θ as the primary unknown.

2.2 Local cardiac coordinate system {n,c,z}

To establish a local cardiac coordinate system $\{\mathbf{n},\mathbf{c},\mathbf{z}\}$, we identify the normal $\mathbf{n}$, circumferential $\mathbf{c}$ and longitudinal $\mathbf{z}$ directions at each node (Tsamis et al. 2011). First, we assign vector $\mathbf{z}$ pointing along the long axis of the heart. Second, we calculate the nodal normals $\mathbf{n}$ using an area-weighted face-normal averaging algorithm commonly used in computer graphics (Max 1999). We calculate the facet normals to each surface triangle by taking the cross product of two edge vectors of the corresponding facet. We then calculate the nodal normal $\mathbf{n}$ as average over all facet normals connected at the particular node. Since the magnitude of the cross product is proportional to the area of the corresponding facet, our nodal normal is automatically area averaged. Third, we calculate the circumferential direction $\mathbf{c}$ as the weighted cross product of the longitudinal and normal vectors $\mathbf{z}$ and $\mathbf{n}$ (Tsamis et al. 2012),

$$\mathbf{c} = \phi[\mathbf{z}\times\mathbf{n}]. \tag{3}$$

To ensure a proper circumferential orientation we weigh the cross product with the orientation index ϕ,

$$\phi = \bar{\phi} = \begin{cases} +1 & \text{on} \quad \partial\mathcal{B}_{\phi^+} \\ -1 & \text{on} \quad \partial\mathcal{B}_{\phi^-} \end{cases}, \tag{4}$$

which is positive on the epicardium and the right septal endocardium $\partial\mathcal{B}_{\phi^+}$ and negative on the left endocardium and right free wall endocardium $\partial\mathcal{B}_{\phi^-}$.

2.3 Nodal fibre and sheet orientations f and s

We can now assign the fibre and sheet orientations $\mathbf{f}$ and $\mathbf{s}$ as indicated in Figure 1. In particular, we assume that fibres $\mathbf{f}$ at the inner and outer surfaces of the heart lie within the tangent plane to the corresponding surface. To begin, we calculate the outward pointing normal $\mathbf{n}_{\text{cz}}$ with respect to the local cz-plane,

$$\mathbf{n}_{\text{cz}} = \mathbf{c}\times\mathbf{z}. \tag{5}$$

Although we could, in principle, assign any given sheet angle β to define the sheet direction, here, without loss of generality, we select the sheet normal $\mathbf{s}$ to be aligned with the outward facing nodal normal,

$$\mathbf{s} = \text{sign}(\mathbf{n}_{\text{cz}}\cdot\mathbf{n})\mathbf{n}. \tag{6}$$

To specify the fibre angle with respect to the horizontal plane, we assume that all fibres within the epicardium and right septal endocardium are inclined with -70° and all fibres within the left endocardium and right free wall endocardium are inclined with 80° (Nielsen et al. 1991),

$$\alpha = \begin{cases} -70^\circ & \text{on} \quad \partial\mathcal{B}_{\phi^+} \\ +80^\circ & \text{on} \quad \partial\mathcal{B}_{\phi^-} \end{cases} \tag{7}$$

We then construct the projection $\mathbf{p}$ of the fibre direction $\mathbf{f}$ on the cz-plane corresponding to the fibre orientation angle α with respect to the circumferential

direction **c**,

$$\mathbf{p} = \text{proj}(\mathbf{f}) = \cos(\alpha)\mathbf{c} + \sin(\alpha)\mathbf{z}. \tag{8}$$

Finally, we rotate the fibre direction **p** from the cz-plane back into the sheet plane tangent to the surface,

$$\mathbf{f} = [-\mathbf{p}\cdot\mathbf{s}]\mathbf{n}_{\text{cz}} + [\mathbf{n}_{\text{cz}}\cdot\mathbf{s}]\mathbf{p}. \tag{9}$$

At this point, we have assigned fibre and sheet directions **f** and **s** to each surface node on $\partial\mathcal{B}_{\phi^+}$ and $\partial\mathcal{B}_{\phi^-}$, which we can then normalise for the sake of convenience. To obtain smooth fibre distributions, we interpolate **f** and **s** into the cardiac domain $\mathcal{B}$ by interpreting each vector component as scalar-valued feature θ and solve the corresponding Poisson problem (1) a total of six times. Theoretically, to increase computational efficiency, we could interpolate the two first components of **f** and **s**, e.g. the components in the x- and y-direction, and then determine the third vector component, the component in the z-direction, through normalisation. This would reduce the computational cost to solving the Poisson problem a total of four times, plus calculating the third vector component for both **f** and **s**. Table 1 summarises the fibre and sheet interpolation algorithm for a given heart mesh and given fibre angles α on the cardiac surfaces.

Remark 1. If we preferred the sheet directions to be orthonormal, we could first interpolate the normal directions **n** using the Poisson interpolation. Then, we would create sheet normals $\tilde{\mathbf{s}}$ orthogonal to the fibre direction **f**.

$$\tilde{\mathbf{s}} = [\mathbf{f}\times\mathbf{s}]\times\mathbf{f}. \tag{10}$$

We recommend reprojecting the sheet normal directions **s** instead of the fibre directions **f** because of the no-contact assumption.

Remark 2. Our algorithm is designed to interpolate sparse vector fields across a given domain. The user-defined constraints, which serve as Dirichlet boundary conditions, do not necessarily have to be prescribed at the epicardial and endocardial surfaces $\partial\mathcal{B}_{\phi^+}$ and $\partial\mathcal{B}_{\phi^-}$, but could potentially also be prescribed anywhere inside the domain.

3. Results

To illustrate our algorithm, we analyse four benchmark problems. First, we use an idealised geometry compatible with prolate spheroid coordinate systems to compare our method against an analytically assigned fibre orientation. Second, we utilise a human heart mesh to demonstrate how our algorithm works on a real patient-specific geometry. Third, we analyse the sensitivity of the fibre distribution with respect to randomly distributed boundary conditions. Fourth, we perform a second sensitivity analysis, however, now with respect to uniformly distributed boundary conditions.

3.1 Generic bi-ventricular heart model

Figure 2 shows the Poisson interpolation providing a smooth continuum description across the pre-defined boundary sets. We observe a spiral-like fibre orientation in the left endocardium, which contributes to the characteristic torsional motion in the left ventricle.

Figure 3 shows the fibres and sheet plane normals at slices towards the top, middle and bottom of the ventricles. Even the fibre orientation around the apex, a challenging region for fibre assignment, seems reasonable and smooth. In summary, our feature-based Poisson interpolation agrees excellently with the analytically assigned fibre orientations of the generic bi-ventricular heart model (Göktepe and Kuhl 2010).

Table 1. Algorithm for creating smoothly varying fibre and sheet orientations f and s within a human heart, for a given mesh and prescribed fibre angles α on the surfaces of the heart.

Identify epicardial and endocardial surfaces $\partial\mathcal{B}_{\phi^+}$ and $\partial\mathcal{B}_{\phi^-}$
For all nodes on $\partial\mathcal{B}_{\phi^+}$ and $\partial\mathcal{B}_{\phi^-}$ Assign local cardiac coordinate system {**n**,**c**,**z**} (3) Assign sheet plane normal **s** (6) Assign fibre angles α with respect to horizontal circumferential direction **c** (7) Calculate projection **p** of the fibre direction (8) Calculate fibre direction **f** from rotation of projection into sheet plane (9)
Solve Poisson equation for each component of **f** and **s** interpreted as feature θ (1) using **f** and **s** on $\partial\mathcal{B}_{\phi^+}$ and $\partial\mathcal{B}_{\phi^-}$ as Dirichlet boundary conditions (2)
Collect and normalise the three components of **f** and **s** at each node
[*Optional*] Correct sheet normals such that **f** and $\tilde{\mathbf{s}}$ form an orthonormal basis (10) [*Optional*] Interpolate **f** and $\tilde{\mathbf{s}}$ to integrate points or element centroids

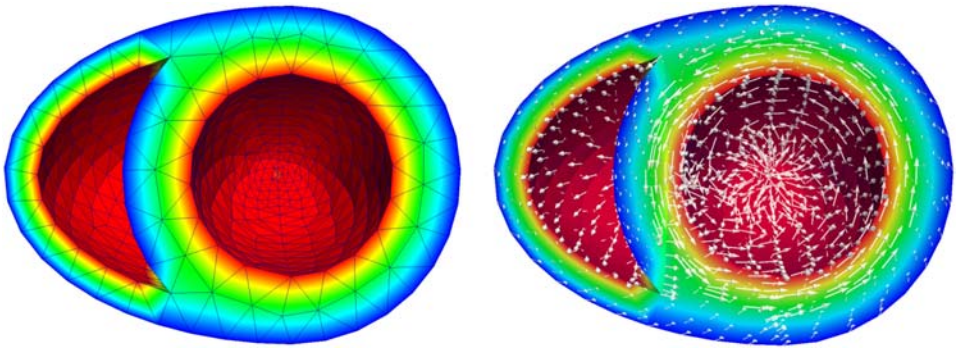

Figure 2. (Left) Poisson interpolation results of fibre orientation angle with respect to circumferential fibre. Epicardial and right ventricular septal surfaces are assigned as $-70°$, whereas the endocardial surfaces are assigned as $80°$ as boundary conditions. (Right) Resulting interpolated fibre directions throughout the heart.

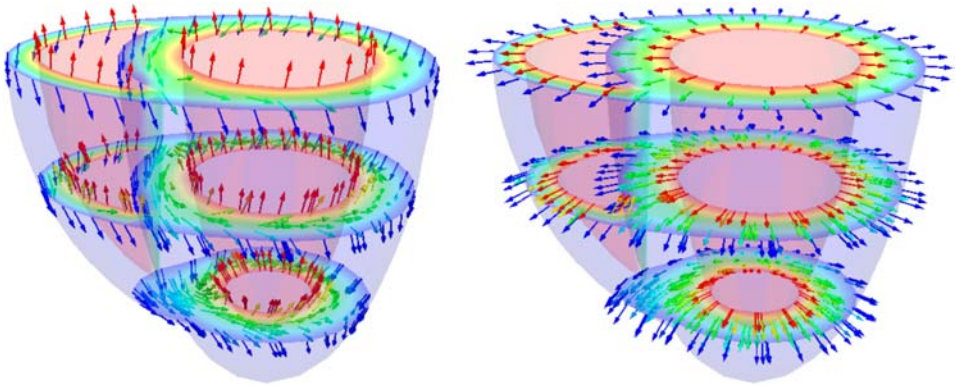

Figure 3. (Left) Fibre directions at various slices in the heart are shown. (Right) The normal directions at the corresponding slices are shown. The colours at each point of the cross-sectional slices correspond to the fibre angle orientation with blue representing $-70°$ and red representing $+80°$ (colour online).

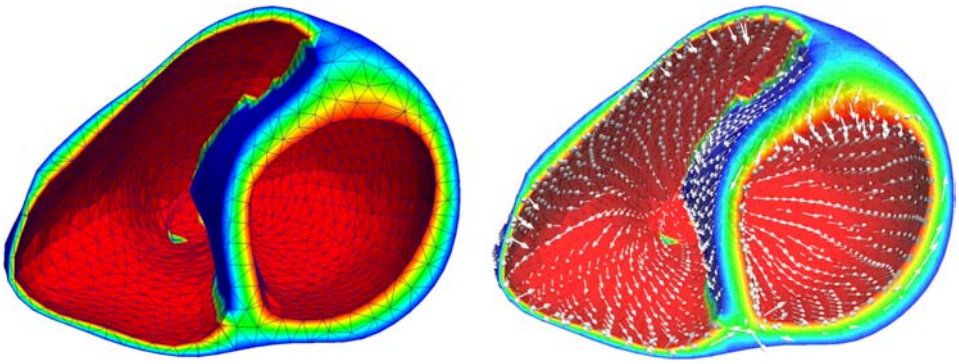

Figure 4. (Left) Poisson interpolation results of fibre orientation angle with respect to circumferential fibre. Epicardial and right ventricular septal surfaces are assigned as $-70°$, whereas the endocardial surfaces are assigned as $80°$ as boundary conditions. (Right) Resulting interpolated fibre directions throughout the heart.

3.2 Patient-specific human heart model

Figure 4 shows the results for the patient-specific heart model generated from magnetic resonance images (Kotikanyadanam et al. 2010; Wong et al. 2012a). Similar to the generic idealised heart, the Poisson interpolation provides a smooth continuum description across the pre-defined boundary sets.

Figure 5 illustrates the resulting fibre and sheet interpolations. The solution of the Poisson problem creates a smooth interpolation through the thickness of the

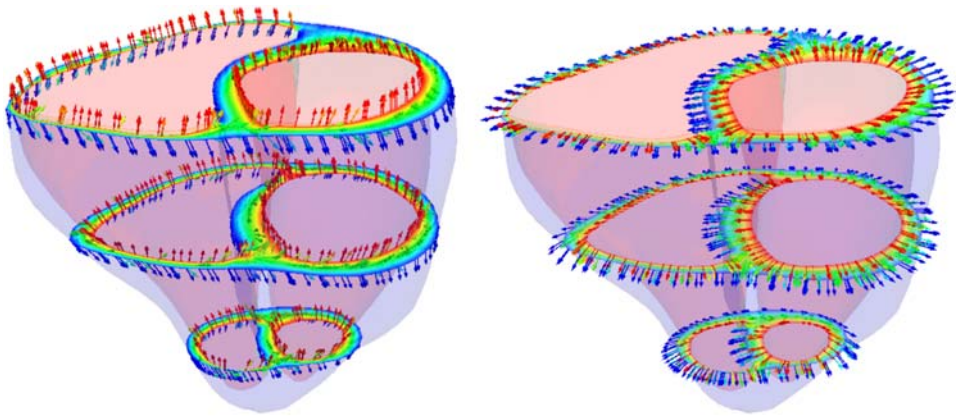

Figure 5. (Left) Fibre directions at various slices in the heart are shown. (Right) The normal directions at the corresponding slices are shown.

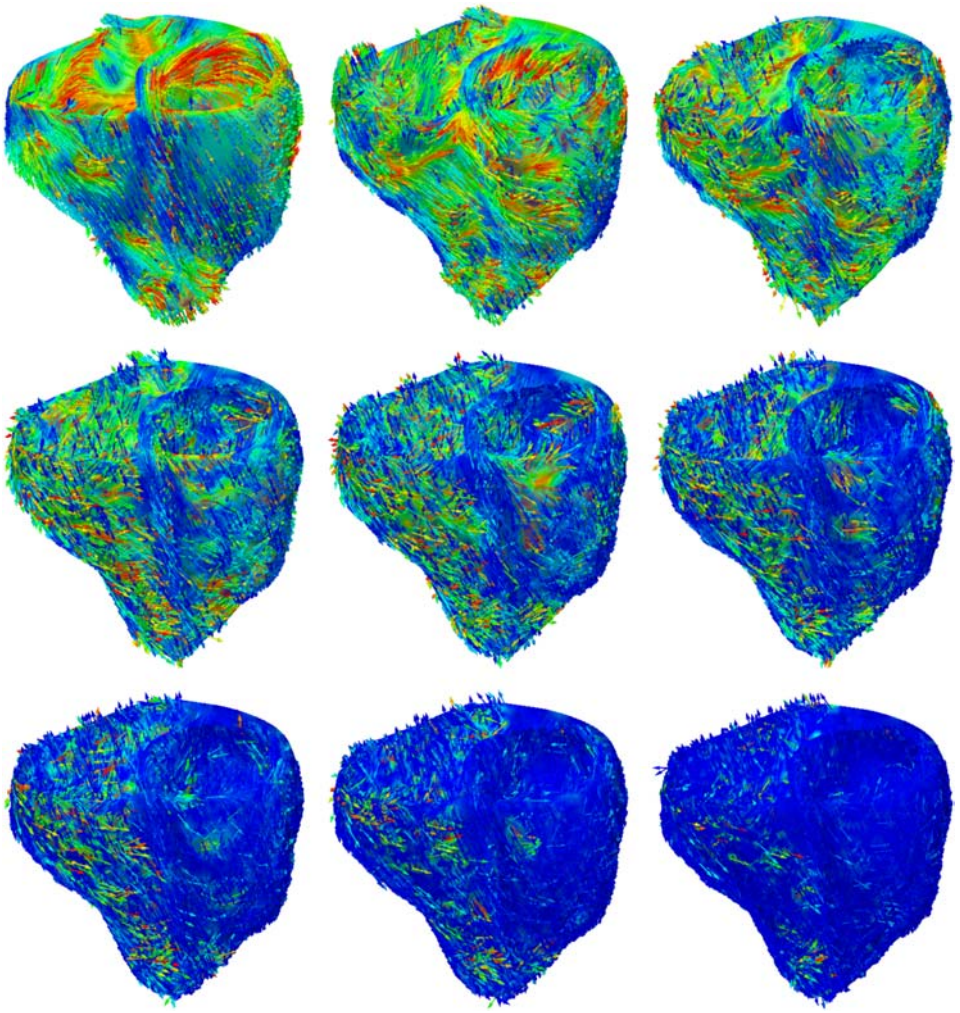

Figure 6. Representative figures of angle fibre error given random subsets of boundary conditions for the fibre interpolation algorithm. Fibres highlighted in blue have no error (0°) whereas red fibres are closer to perpendicular (90°). Increasing sizes of random subsets are chosen and are shown starting from 10% (top left), 20% (top centre), 30% (top right), 40% (left), 50% (centre), 60% (right), 70% (bottom left), 80% (bottom centre) and 90% (bottom right) (colour online).

myocardium for both fibre directions and sheet plane normals. Again, we can observe the characteristic torsion-inducing fibre orientation in both ventricles. Like the generic model, the fibre distribution near the apex is smooth and continuous. In summary, the algorithm is capable of creating smooth fibre and sheet interpolations on arbitrary patient-specific geometries, even in geometrically challenging regions such as the apex.

3.3 Sensitivity analysis for randomly distributed boundary conditions

Since our fibre interpolation algorithm is framed as a boundary value problem with user-defined constraints, we next perform numerical tests to determine the relative sensitivity of the overall fibre distribution with respect to changes in the boundary conditions. In our first set of tests, we select random subsets of our boundary conditions ranging from 10% to 100% of all boundary conditions at the surface nodes. These tests serve to determine the amount of error in angle distributions we might expect from a random, and possibly poor spatial uniformity of measurements. We define the angle error $e^{\angle}$ as

$$e^{\angle} = |\arccos(\mathbf{f} \cdot \mathbf{f}^{\text{int}})|, \tag{11}$$

where $\mathbf{f}$ and $\mathbf{f}^{\text{int}}$ are the exact and interpolated fibre orientation.

Figure 6 illustrates representative fibre interpolation errors from 10%, top left, to 90%, bottom right, of all possible boundary conditions used. Since we have chosen the random subsets of the boundary conditions randomly for each ratio, we expect the angle error to be more or less randomly distributed across the mesh. As the subset of assigned boundary condition grows from 10% to 90%, the angle error decreases.

Figure 7 displays the average angle error for varying random boundary condition ratios from 10% to 100%. As a rule of thumb, when using randomly distributed boundary conditions, to obtain an angle error of 10% or less on average, we have to prescribe at least 70% of the surface nodes as boundary conditions.

3.4 Sensitivity analysis for uniformly distributed boundary conditions

Finally, since real fibre data extracted from histology or diffusion tensor imaging are typically acquired in a spatially uniform manner, we performed a mesh refinement test. We generated a coarse patient-specific mesh of 4563 nodes (Kotikanyadanam et al. 2010) and refined it recursively twice using edge bi-section subdivision. For each of the three meshes, we performed a Poisson interpolation to generate fibre orientations and assigned

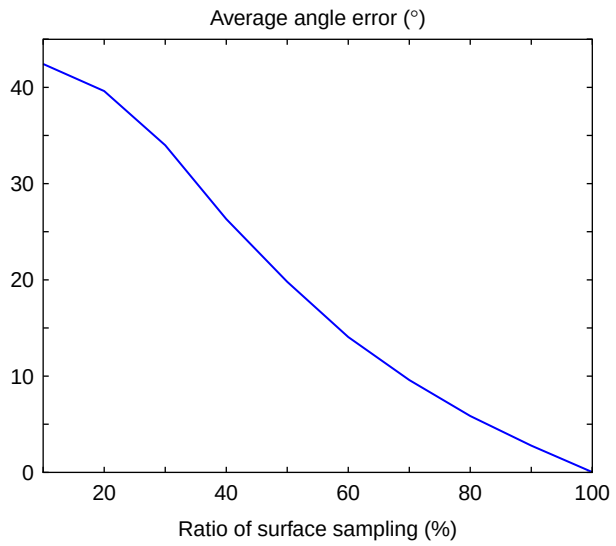

Figure 7. Average angle error when 10–100% of the surface nodes used as boundary conditions to generate fibre orientation distribution.

boundary conditions only to the original 4563 nodes. We then calculated the angle error (13) between the two subdivided meshes averaged over all nodes. Table 2 summarises the generating parameters and mesh data.

Figure 8 illustrates the results of the mesh refinement study. With spatially uniform subsets of the boundary conditions, in contrast to the previous problem, we observe that the error is less than 10% for only 6.25% of the surface nodes prescribed as boundary conditions.

Figure 9 illustrates the fibre angle error in first subdivision mesh compared with second subdivision mesh. When using uniformly distributed boundary conditions, most fibres display an error of 20% or less. This indicates that our algorithm works best when interpolating uniformly distributed features across the heart.

Table 2. Table of parameters for random and subdivision examples.

Surfaces	Fibre angle (°)	
Epicardium, right septal wall, $\partial\mathcal{B}_{\phi^+}$	−70	
Left endocardium, right free wall, $\partial\mathcal{B}_{\phi^-}$	+80	
Subdivision	**No. of surface nodes**	**No. of total nodes**
Initial mesh	3839	4563
1st Subdivision	15,350	28,639
2nd Subdivision	61,394	198,041
Average angle error	9.965°	

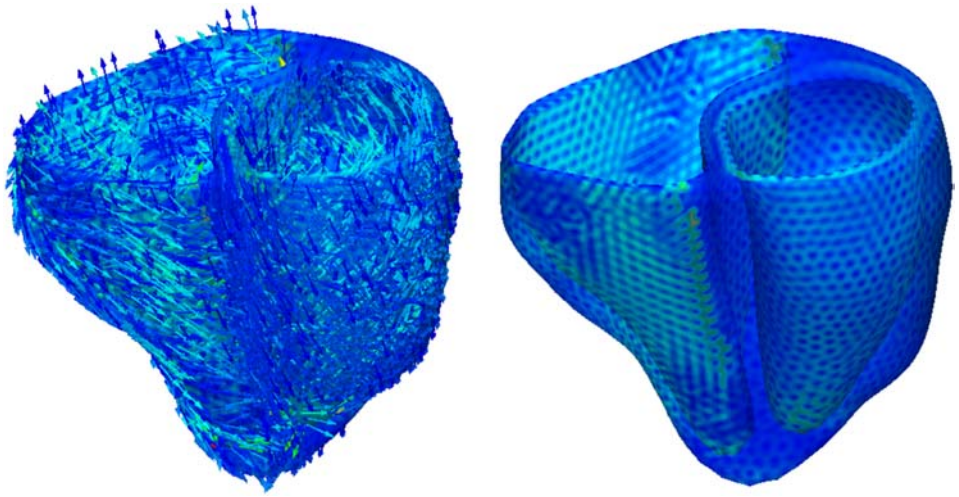

Figure 8. (Left) Fibre direction colour coded by angle error. (Right) Fibre angle error over the heart without fibres. Small hexagonal patterns are formed, because the nodes at the coarsest mesh are used as the boundary condition set, and therefore the new nodes on the surfaces are not part of this boundary condition set (colour online).

4. Discussion

We believe that the results from the previous section demonstrate the advantages of a geometrical approach, compared to a mathematical approach, when generating fibre orientation maps for computational human heart models. The proposed method is able to reproduce fibre orientations for given fibre angles on an idealised geometry (Nielsen et al. 1991). As the analytical fibre distribution elegantly enforces a linear interpolation across the thickness of the ellipsoidal ventricle (Göktepe and Kuhl 2010), a Poisson interpolation with uniform properties on the same geometry generates identical results.

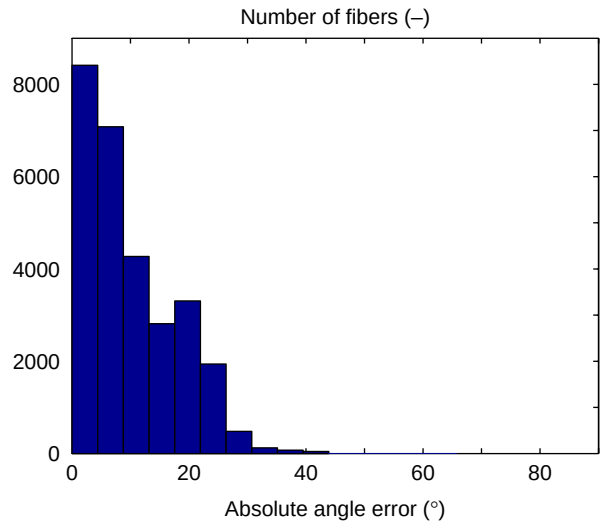

Figure 9. Histogram of fibre angle error in first subdivision mesh compared with second subdivision mesh. The histogram is organised into bins of 5° error.

However, by using our geometrical approach, we can avoid singularities in the septum and at the apex inherent to the mathematical approach by directly controlling the fibre orientation when **n** and **z** are perfectly aligned.

Our geometrical approach allows us to easily transfer the elegance of the mathematical approach to arbitrary patient-specific geometries (Kotikanyadanam et al. 2010; Wong et al. 2011). For finite element models of anisotropic electrical conduction (Chen et al. 2012; Dal et al. 2012) or anisotropic cardiac mechanics (Göktepe et al. 2010, 2011; Wong et al. 2012b), our geometrical approach is convenient since its results can immediately feed into a finite element analysis. The Poisson interpolation is easy, fast and robust at various mesh granularities.

Here, we have chosen linear tetrahedral elements since they are closely related to concepts of discrete exterior calculus used in computer graphics to interpolate surface features on arbitrary geometries (Fisher et al. 2007; Hauret et al. 2007). In addition, tetrahedral elements are widely used and easy to understand. However, the proposed concept is easily expandable to hexahedral elements. In fact, it is even compatible with cubic Hermitian elements (Nielsen et al. 1991), which already contain the necessary information regarding surface normals, sheet direction and tangent direction.

Another advantage of solving the Poisson interpolation with finite element solvers is that the finite element method ensures the best approximating solution if the governing differential equation is linear. This has some interesting implications. For example, it means that the method presented can also properly account for non-constant value boundary conditions, which may occur if more detailed fibre orientation measurements are available. Given experimental measurements, our algorithm returns the

best approximating solution that matches the fibre orientation for different mesh refinement levels. To further fine-tune control of the fibre orientation profile, the finite element method allows us to easily integrate additional constraints.

Previously, least squares methods have been proposed to generate fibre orientation distributions (Costa et al. 1996). However, there are fundamental differences between the finite element method and the least squares methods. The least squares approach will try to find the solution that most closely resembles the measured fibre orientation (Toussaint et al. 2010a). As such, it strongly depends on the character of the interpolating shape functions and on the underlying discretisation scheme. The finite element method, however, enforces user-defined fibre orientations at the specific nodes. It satisfies the Dirichlet boundary conditions in a strong sense, and determines the best approximating fibre orientation at all other nodes. However, least squares methods and this finite element method are not exclusive approaches and can be used in tandem when necessary. For example, least squares methods can be used to smoothen out the distribution on surfaces, which our finite element method can then interpolate through the thickness.

Perhaps the most exciting and most useful application of our feature-based Poisson interpolation compared with analytical and least squares approaches is the ability to fill in gaps when there is lack of experimental data. Since it is known that the heart has an organised fibre orientation and it may be significantly easier to measure the surfaces of tissue rather than the inner layers, our method can provide a reasonable approximation using a combination of observable results and a more algorithmically methodical approach. Even if we only measure a relatively sparse, yet spatially uniform, set of fibre directions, either histologically (Ennis et al. 2008) or from diffusion tensor imaging (Toussaint et al. 2010b), fibre diffusion can fill in the gaps and create a reasonable and smooth solution as shown in Figure 8. In addition, we can easily integrate experimental data at no-nodal points, e.g. from magnetic resonance imaging (Böl et al. 2011), using constraint boundary conditions.

The proposed method provides a variety of natural extensions and generalisations that may be of interest to the biomechanics community. For example, we could easily apply the underlying concept to other muscular tissues such as skeletal muscle (Böl and Reese 2008; Lu et al. 2011; Zöllner et al. 2012), or to collagenous structures in other biological tissues. If we assume that the transitioning nature between the two surfaces in a body is not linear, we could vary the diffusion tensor at varying points within the body to match the description accurately. Although the heart's transmural fibre orientation transition is almost linear (Ennis et al. 2008), by varying the transmural or in-plane conductivity, we could potentially approximate nonlinear transmural and regional fibre variations. Likewise, the fibre orientation distribution can be more carefully adjusted and tuned by possibly using inequality constraints, which might be more physiological. Another possible extension would be using noisy source terms with the finite element model to account for biological variability. Along a similar vein, fibre interpolation can be used as a tool to generate smoothly varying fibre fields with random defects to represent diseased tissue conditions (Schmitt et al. 2009), similar to the bottom row of Figure 7. We could generate and control the amount of disorganisation within the fibre structure, and virtually investigate the impact of different clinical therapies on electrical and mechanical function in cases in which the fibre orientation is globally irregular or locally distorted.

5. Conclusion

We have presented a novel Poisson interpolation-based approach to create fibre orientation maps in real patient-specific heart geometries. The algorithm makes creative use of existing and common linear finite element programs for diffusion or thermal problems. Adopted from computer graphics, the underlying concept is based on diffusing a defined subset of fibre orientations throughout the domain of interest to create smoothly interpolating fields. In the finite element setting, this subset is simply treated as Dirichlet boundary condition and enforced in a strong sense. Here, we have shown the application of the Poisson interpolation scheme to create fibre orientation maps across the heart, but the general concept can easily be applied to other arbitrarily shaped biological tissues with known organised fibre orientations. We have shown that the algorithm does generally work for both arbitrarily and uniformly distributed input data. However, our interpolation errors were significantly lower for uniform distributions. In summary, the proposed method is computationally efficient, robust and easy to solve. It is immediately transformative to generate smoothly interpolated fields in experimental and clinical settings, in which data-sets are sparse but uniformly distributed.

Acknowledgements

We thank Dr Euan Ashley for providing the patient-specific magnetic resonance image and Anton Dam, Rebecca Taylor, Daniel Burkhart and Alexander Zöllner for their help in creating the finite element mesh. Jonathan Wong was supported by the Sang Samuel Wang Stanford Graduate Fellowship. Ellen Kuhl was supported by the NSF CAREER award CMMI 0952021, by the NSF INSPIRE grant 1233054 and by the NIH grant U54 GM072970.

References

Arts T, Costa KD, Covell JW, McCulloch AD. 2001. Relating myocardial laminar architecture to shear strain and muscle fiber orientation. Am J Physiol Heart Circ Physiol. 280(5):H2222–H2229.

Böl M, Reese S. 2008. Micromechanical modelling of skeletal muscles based on the finite element method. Comput Methods Biomech Biomed Eng. 11(5):489–504.

Böl M, Sturmat M, Weichert C, Kober C. 2011. A new approach for the validation of skeletal muscle modeling using MRI data. Comput Mech. 47:591–601.

Chen MQ, Wong J, Kuhl E, Giovangrandi L, Kovacs GTA. 2012. Characterization of electrophysiological conduction in cardiomyocyte co-cultures using co-occurrence analysis. Comput Methods Biomech Biomed Eng., doi: 10.1080/10255842.2011.615310.

Costa KD, Hunter PJ, Wayne JS, Waldman LK, Guccione JM, McCulloch AD. 1996. A three-dimensional finite element method for large elastic deformations of ventricular myocardium: II – prolate spheroidal coordinates. J Biomech Eng. 118(4):464–472.

Dal H, Göktepe S, Kaliske M, Kuhl E. 2012. A fully implicit finite element method for bidomain models of cardiac electrophysiology. Comput Methods Biomech Biomed Eng. 15:645–656.

Ennis DB, Nguyen TC, Riboh JC, Wingström L, Harrington KB, Daughters GT, Ingels NB, Miller DC. 2008. Myofiber angle distributions in the ovine left ventricle do not conform to computationally optimized predictions. J Biomech Eng. 41:3219–3224.

Fisher M, Schröder P, Desbrun M, Hoppe H. 2007. Design of tangent vector fields. ACM Trans Graph. 26:56–64.

Geerts L, Bovendeerd P, Nicolay K, Arts T. 2002. Characterization of the normal cardiac myofiber field in goat measured with MR-diffusion tensor imaging. Am J Physiol Heart Circ Physiol. 283(1):H139–H145.

Göktepe S, Kuhl E. 2010. Electromechanics of the heart – a unified approach to the strongly coupled excitation-contraction problem. Comput Mech. 45:227–243.

Göktepe S, Abilez OJ, Parker KK, Kuhl E. 2010. A multiscale model for eccentric and concentric cardiac growth through sarcomerogenesis. J Theor Biol. 265:433–442.

Göktepe S, Acharya SNS, Wong J, Kuhl E. 2011. Computational modeling of passive myocardium. Int J Numerical Methods Biomed Eng. 27:1–12.

Hauret P, Kuhl E, Ortiz M. 2007. Diamond elements: a finite-element/discrete-mechanics approximation scheme with guaranteed optimal convergence in incompressible elasticity. Int J Numerical Methods Eng. 72:253–294.

Kotikanyadanam M, Göktepe S, Kuhl E. 2010. Computational modeling of electrocardiograms – a finite element approach towards cardiac excitation. Int J Numerical Methods Biomed Eng. 26:524–533.

Kumar V, Abbas AK, Fausto N. 2005. Robbins and Cotran pathologic basis of disease. Philadelphia: Elsevier Saunders.

Libby P, Bonow RO, Mann DL, Zipes DP. 2007. Braunwald's heart disease. Philadelphia: Saunders.

Lu YT, Zhu HX, Richmond S, Middleton J. 2011. Modelling skeletal muscle fibre orientation arrangement. Comput Methods Biomech Biomed Eng. 14(12):1079–1088.

Max N. 1999. Weights for computing vertex normals from facet normals. J Graph Tools. 4:1–6.

Nielsen PM, Le Grice IJ, Smaill BH, Hunter PJ. 1991. Mathematical model of geometry and fibrous structure of the heart. Am J Physiol Heart Circ Physiol. 260(4):H1365–H1378.

Opie LH. 2003. Heart physiology: from cell to circulation. Philadelphia: Lippincott Williams & Wilkins.

Schmitt B, Fedarava K, Falkenberg J, Rothaus K, Bodhey NK, Reischauer C, Kozerke S, Schnackenburg B, Westermann D, Lunkenheimer PP et al., 2009. Three-dimensional alignment of the aggregated myocytes in the normal and hypertrophic murine heart. J Appl Physiol. 107:921–927.

Sosnovik DE, Wang R, Dai G, Wang T, Aikawa E, Novikov M, Rosenzweig A, Gilbert RJ, Wedeen VJ. 2009. Diffusion spectrum MRI tractography reveals the presence of a complex network of residual myofibers in infarcted myocardium. Circ: Cardiovasc Imaging. 2(3):206–212.

Streeter DD, Hanna WT. 1973. Engineering mechanics for successive states in canine left ventricular myocardium: II Fiber angle and sarcomere length. Circ Res. 33(6):656–664.

Takayama K, Ashihara T, Ijiri T, Igarashi T, Haraguchi R, Nakazawa K. 2008. A sketch-based interface for modeling myocardial fiber orientation that considers the layered structure of the ventricles. J Physiol Sci. 58(7):487–492.

Toussaint N, Stoeck CT, Kozerke S, Sermesant M, Batchelor PG. 2010a. *In vivo* human 3D cardiac fibre architecture: reconstruction using curvilinear interpolation of diffusion tensor images. In: Proceedings Medical Image Computing and Computer Assisted Intervention. LNCS, Beijing, Canada: Springer.

Toussaint N, Stoeck CT, Sermesant M, Kozerke S, Batchelor PG. 2010b. Three-dimensional prolate spheroidal extrapolation for sparse DTI of the *in vivo* heart. In: Book of Abstracts of the International Society in Magnetic Resonance in Medicine. Sweden: Stockholm.

Tsamis A, Bothe W, Kvitting JP, Swanson JC, Miller DC, Kuhl E. 2011. Active contraction of cardiac muscle: *in vivo* characterization of mechanical activation sequences in the beating heart. J Mech Behav Biomed Mater. 4:1167–1176.

Tsamis A, Cheng A, Nguyen TC, Langer F, Miller DC, Kuhl E. 2012. Kinematics of cardiac growth: *in vivo* characterization of growth tensors and strains. J Mech Behav Biomed Mater. 8:165–177.

Wong J, Göktepe S, Kuhl E. 2011. Computational modeling of electrochemical coupling: a novel finite element approach towards ionic models for cardiac electrophysiology. Comput Methods Appl Mech Eng. 200:3139–3158.

Wong J, Abilez OJ, Kuhl E. 2012a. Computational optogenetics: a novel continuum framework for the photoelectrochemistry of living systems. J Mech Phys Solids. 60:1158–1178.

Wong J, Göktepe S, Kuhl E. 2012b. submitted for publication Computational modeling of chemo-electro-mechanical coupling: a novel implicit monolithic finite element approach.

Yang F, Zhu YM, Magnin IE, Luo JH, Croisille P, Kingsley PB. 2012. Feature-based interpolation of diffusion tensor fields and application to human cardiac DT-MRI. Med Image Anal. 16(2):459–481.

Zöllner AM, Abilez OJ, Böl M, Kuhl E. 2012. Stretching skeletal muscle – chronic muscle lengthening through sarcomerogenesis. PLoS ONE. 7(10):e45661.